ARTICLE

doi:10.1038/nature14583

Progesterone receptor modulates ERα action in breast cancer

Hisham Mohammed[1], I. Alasdair Russell[1], Rory Stark[1], Oscar M. Rueda[1], Theresa E. Hickey[2], Gerard A. Tarulli[2], Aurelien A. A. Serandour[1], Stephen N. Birrell[2], Alejandra Bruna[1], Amel Saadi[1], Suraj Menon[1], James Hadfield[1], Michelle Pugh[1], Ganesh V. Raj[3], Gordon D. Brown[1], Clive D'Santos[1], Jessica L. L. Robinson[1], Grace Silva[4], Rosalind Launchbury[1], Charles M. Perou[4], John Stingl[1], Carlos Caldas[1,5,6], Wayne D. Tilley[2]§ & Jason S. Carroll[1]§

Progesterone receptor (PR) expression is used as a biomarker of oestrogen receptor-α (ERα) function and breast cancer prognosis. Here we show that PR is not merely an ERα-induced gene target, but is also an ERα-associated protein that modulates its behaviour. In the presence of agonist ligands, PR associates with ERα to direct ERα chromatin binding events within breast cancer cells, resulting in a unique gene expression programme that is associated with good clinical outcome. Progesterone inhibited oestrogen-mediated growth of ERα$^+$ cell line xenografts and primary ERα$^+$ breast tumour explants, and had increased anti-proliferative effects when coupled with an ERα antagonist. Copy number loss of *PGR*, the gene coding for PR, is a common feature in ERα$^+$ breast cancers, explaining lower PR levels in a subset of cases. Our findings indicate that PR functions as a molecular rheostat to control ERα chromatin binding and transcriptional activity, which has important implications for prognosis and therapeutic interventions.

There is compelling evidence that inclusion of a progestogen as part of hormone replacement therapy increases the risk of breast cancer, implying that PR signalling can contribute towards tumour formation[1]. However, the increased risk of breast cancer associated with progestogen-containing hormone replacement therapy is mainly attributed to specific synthetic progestins, in particular medroxyprogesterone acetate (MPA), which is known to also have androgenic properties[2]. The relative risk is not significant when native progesterone is used[3]. In ERα$^+$ breast cancers, PR is often used as a positive prognostic marker of disease outcome[4], but the functional role of PR signalling remains unclear. While activation of PR may promote breast cancer in some women and in some model systems, progesterone treatment has been shown to be antiproliferative in ERα$^+$ PR$^+$ breast cancer cell lines[5–7], and progestogens have been shown to oppose oestrogen-stimulated growth of an ERα$^+$ PR$^+$ patient-derived xenograft[8]. In addition, exogenous expression of PR in ERα$^+$ breast cancer cells blocks oestrogen-mediated proliferation and ERα transcriptional activity[9]. Furthermore, in ERα$^+$ breast cancer patients, PR is an independent predictor of response to adjuvant tamoxifen[10], high levels of PR correlate with decreased metastatic events in early stage disease[11], and administration of a progesterone injection before surgery can provide improved clinical benefit[12]. These observations imply that PR activation in the context of oestrogen-driven, ERα$^+$ breast cancer, can have an anti-tumorigenic effect. In support of this, PR agonists can exert clinical benefit in ERα$^+$ breast cancer patients that have relapsed on ERα antagonists[13].

Breast cancers are typically assessed for ERα, PR and HER2 expression to define histological subtype and guide treatment options. PR is an ERα-induced gene[14] and ERα$^+$ PR$^+$ HER2$^-$ tumours tend to have the best clinical outcome because PR positivity is thought to reflect a tumour that is driven by an active ERα complex and therefore likely to respond to endocrine agents such as tamoxifen or aromatase inhibitors[10,15]. While ERα$^+$ PR$^+$ tumours have a better clinical outcome than ERα$^+$ PR$^-$ tumours[4], clinical response to ERα antagonists can vary, even among tumours with similar ERα and PR status[15,16], and recent evidence suggests that PR may be prognostic, but not predictive[17]. Some ERα$^+$ PR$^-$ tumours that are resistant to one class of ERα antagonists gain clinical benefit from another class, suggesting that in a subset of ERα$^+$ PR$^-$ breast cancers, the lack of PR expression does not reflect a non-functional ERα complex. It has been proposed that the non-functional ERα complex theory cannot completely explain PR negativity[18]. An alternative hypothesis is that other factors contribute to the loss of PR expression, which consequently influences breast tumour responses to ERα target therapies.

PR is recruited to the ERα complex

Given the controversial and complex interplay between the ERα and PR pathways in breast cancer, we explored the possible functional crosstalk between these two transcription factors and the implications for clinical prognosis in ERα$^+$ disease. Ligand-activated ERα and PR protein complexes were purified to ascertain interplay between these two transcription factors. Asynchronous ERα$^+$ PR$^+$ MCF-7 and T-47D breast cancer cells were grown in stable isotope labelling by amino acids in cell culture (SILAC) growth media, which contains sufficient oestrogen to elicit maximal ERα binding to chromatin[19]. Oestrogen treatment is required to induce detectable levels of PR in MCF-7 cells, but not in T-47D cells[20]. The two cell lines were subsequently treated with vehicle or one of two progestogens: native progesterone or the synthetic progestin R5020. Cells were cross-linked following hormone treatment and endogenous PR was immunopurified followed by mass spectrometry, using a technique we recently developed called RIME (rapid immunoprecipitation mass

[1]Cancer Research UK Cambridge Institute, University of Cambridge, Robinson Way, Cambridge CB2 0RE, UK. [2]Dame Roma Mitchell Cancer Research Laboratories and the Adelaide Prostate Cancer Research Centre, School of Medicine, Hanson Institute Building, University of Adelaide, Adelaide, South Australia 5005, Australia. [3]Department of Urology, University of Texas, Southwestern Medical Center at Dallas, Dallas, Texas 75390, USA. [4]Lineberger Comprehensive Cancer Center, University of North Carolina at Chapel Hill, 450 West Drive, CB7295, Chapel Hill, North Carolina 27599, USA. [5]Cambridge Breast Unit, Addenbrooke's Hospital, Cambridge University Hospital NHS Foundation Trust and NIHR Cambridge Biomedical Research Centre, Cambridge CB2 2QQ, UK. [6]Cambridge Experimental Cancer Medicine Centre, Cambridge CB2 0RE, UK.
§These authors jointly supervised this work.

spectrometry of endogenous proteins)[21]. Under oestrogenic conditions, progesterone treatment induced an interaction between PR and ERα in the MCF-7 and T-47D cell lines, in support of previous findings showing a physical interaction between these two nuclear receptors[22]. In addition to ERα, progesterone treatment induced interactions between PR and known ERα-associated cofactors, including NRIP1, GATA3 and TLE3 (ref. 21) in both cell lines (Fig. 1a). As expected, treatment with natural ligand decreased interaction between PR and chaperone/co-chaperone proteins such as HSP90 and FKBP4/FKBP5 (Fig. 1a). The same findings were observed when R5020 was used as a synthetic ligand (Extended Data Fig. 1). Interestingly, when ERα was purified under the same treatment conditions, PR was the only differentially recruited protein in both cell lines (Fig. 1b). Moreover, the interaction between ERα and known ERα-associated cofactors was not differentially affected by progesterone treatment. A list of all interacting proteins under all experimental conditions is provided in Supplementary Table 1. The progesterone-induced ERα–PR interaction was confirmed by standard co-immunoprecipitation experiments in both MCF-7 and T-47D cells (Fig. 1c). We conclude that activation of PR results in a robust association between PR and the ERα complex. However, it remains unclear what effect this may have on ERα/PR DNA binding or what the primary DNA tethering mechanism may be (Fig. 1d).

Progesterone reprograms ERα binding events

Since PR is a transcription factor, we hypothesized that the progestogen-induced interaction between PR and ERα alters chromatin binding properties of the ERα–cofactor complex. MCF-7 and T-47D cell lines grown in complete (oestrogenic) media were stimulated with progesterone, R5020 or vehicle control for 3 or 24 h, followed by analysis of genome-wide ERα and PR and the co-activator p300 profiles by chromatin immunoprecipitation followed by sequencing (ChIP-seq). p300 deposits the H3K27Ac mark, which is indicative of functional enhancers[23]. We found comparable ERα, PR and p300 binding at 3 h and 24 h (Extended Data Fig. 1 and data not shown) and chose 3 h for the remaining experiments. All ChIP-seq experiments were subsequently repeated in triplicate following 3 h of treatment (sample clustering is provided in Extended Data Fig. 2). Whereas robust ERα binding (29,149 sites in MCF-7 cells and 8,438 sites in T-47D cells) was observed in oestrogenic conditions, limited PR binding events were seen under these conditions (Supplementary Table 2). Treatment with progesterone or the synthetic progestin R5020 in oestrogen-rich media resulted in robust PR recruitment to chromatin, with 46,191 PR binding events observed in T-47D cells with both ligands and 29,554 PR binding events in MCF-7 cells. Using DiffBind to identify differential peaks[24] that occurred following treatment of cells with progesterone or R5020, a rapid and robust redistribution of ERα binding to novel genomic loci was observed (Fig. 2a, b). In T-47D cells, 14,223 ERα binding events were reproducibly gained following 3 h of treatment with progesterone, a finding that was similar following stimulation with R5020, confirming a predictable redistribution of ERα chromatin binding following stimulation of the PR pathway. A similar rapid redirection of ERα was observed in MCF-7 cells after progesterone or R5020 treatment (Extended Data Fig. 1). The ERα sites reprogrammed by progesterone are likely to be functional, as indicated by the global recruitment of the co-activator p300 (Fig. 2b and Extended Data

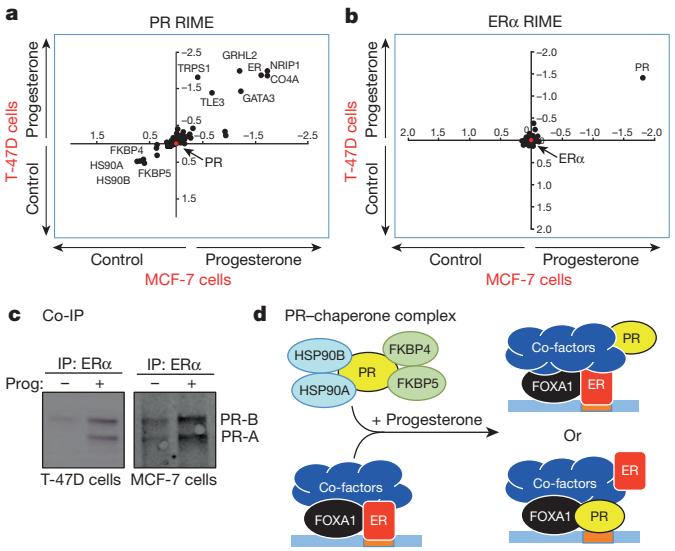

Figure 1 | PR is a novel ERα interacting protein following progesterone treatment. **a**, **b**, MCF-7 and T-47D breast cancer cells were SILAC-labelled, treated with hormones and harvested for RIME (endogenous protein purification-mass spectrometry) of either PR (**a**) or ERα (**b**). Differential proteins identified in both cell lines are plotted and all proteins are provided in Supplementary Table 1. The axes represent log fold change. **c**, Co-immunoprecipitation (IP) validation of PR interactions with ERα. Both PR isoforms interact with ERα. **d**, Model showing possible mechanisms of interplay between PR and ERα (ER)-cofactor complex.

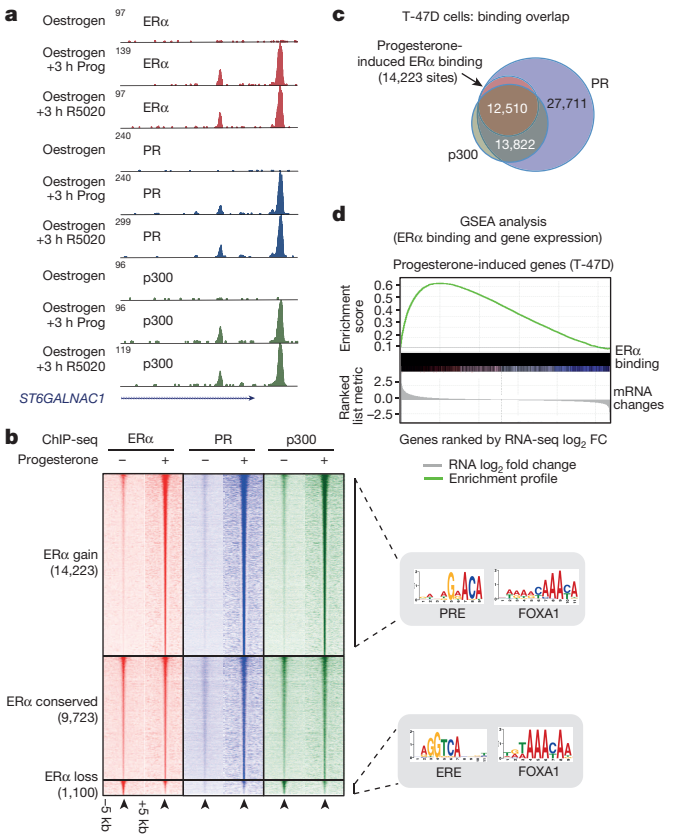

Figure 2 | Progesterone redirects oestrogen-stimulated ERα binding events to novel chromatin loci and transcriptional targets. ChIP-seq for ERα, PR and the co-activator p300 in T-47D cells grown in oestrogen-rich media and treated with progesterone or R5020. **a**, Example binding region of a progesterone/R5020 induced ERα, PR and p300 binding event. **b**, Heat map of ERα, PR and p300 ChIP-seq data from T-47D cells after 3 h of progesterone treatment. The heat map is shown in a horizontal window of ±5 kb. Also shown are the enriched motifs within each category. ERE, oestrogen responsive elements; PRE, progesterone responsive element. **c**, Overlap between progesterone-induced ERα, PR and p300 binding sites, representing only the progestogen-induced ERα binding events. n = three independent biological replicates. **d**, RNA-seq was performed after progesterone or R5020 treatment for 3 h under oestrogenic conditions (control). n = eight independent biological replicates. GSEA analysis was conducted, comparing progestogen-induced transcripts with progestogen-induced ERα binding events within T-47D cells.

Fig. 2). These ERα binding events appear to be mediated by PR, since 99% of the gained ERα binding sites in T-47D cells overlapped with a PR binding event (Fig. 2c) (the overlap in MCF-7 cells was 94%) and motif analysis of the gained ERα sites revealed the presence of progesterone responsive elements, but not oestrogen responsive elements (Fig. 2b). This suggests that PR mediates the interaction between the ERα–PR–p300 complex and DNA. ERα ChIP-seq was repeated in MCF-7 and T-47D cells following hormone deprivation and subsequent treatment with vehicle, oestrogen alone or progesterone alone. Single hormone treatments did not induce the ERα binding events observed under dual hormone conditions (Extended Data Fig. 3), confirming that the ERα reprogramming is dependent on having both receptors activated simultaneously. In addition, Forkhead motifs were enriched at the gained ERα sites and 49% of the gained ERα/PR binding events were shown to overlap with FOXA1 binding (Extended Data Fig. 4), consistent with previous findings showing that PR binding involves the pioneer factor FOXA1 (ref. 25). In keeping with the anti-proliferative effects of progestogens in ERα$^+$ breast cancer cells, analysis of the genes bound by ERα following progesterone treatment revealed enrichment for cell death, apoptosis and differentiation pathways (Supplementary Table 3).

To identify the transcriptional targets of the progestogen-induced ERα binding events, we treated oestrogen-stimulated MCF-7 and T-47D cells with progesterone, R5020 or vehicle for 3 h and performed eight replicates of RNA-seq. In total, 470 genes were differentially regulated by dual treatment with oestrogen and progesterone or R5020 compared to oestrogen alone in both T-47D and MCF7 cell lines (Extended Data Fig. 4). Gene set enrichment analysis (GSEA) analysis revealed a pronounced enrichment of progestogen-induced ERα binding events near genes upregulated by progestogen treatment in the presence of oestrogen (Fig. 2d). Collectively, these findings suggest that the progestogen-mediated changes in ERα binding events are functionally significant, since they co-recruit p300 and lead to new gene expression profiles (Fig. 2d and Extended Data Fig. 4). Importantly, increased expression of a gene signature that results from progesterone-stimulated ERα binding confers good prognosis in a cohort of 1,959 breast cancer patients (Extended Data Fig. 5).

The relative degree of ERα reprogramming and gene expression changes following progesterone treatment was higher in T-47D cells compared to MCF-7 cells (Supplementary Table 2), possibly owing to the differences in PR levels between these two cell lines[20]. We assessed the PR gene (*PGR*) in these cell lines, which revealed copy number gain of the *PGR* gene in T-47D cells and a heterozygous loss of the *PGR* gene in MCF-7 cells (Extended Data Fig. 5). Exogenous expression of PR (both isoforms) in the MCF-7 cell line resulted in growth inhibition (Extended Data Fig. 6), confirming an anti-proliferative role for PR, via modulation of ERα transcriptional activity[9].

Progesterone blocks ERα$^+$ tumour growth

To explore the hypothesis that progesterone stimulation could have beneficial effects on ERα$^+$ tumour growth *in vivo*, we established MCF-7-Luciferase xenografts in *NOD/SCID/IL2Rg*$^{-/-}$ (NSG) mice and exposed the mice to control (that is, no hormone), slow release oestrogen pellets or slow release oestrogen plus standard high concentration progesterone pellets[26]. Ten tumours for each condition were implanted (two tumours per mouse and five mice per condition) and tumour formation was monitored using bioluminescent imaging. After 25 days, in the absence of any hormone, tumours did not grow, but stimulation with oestrogen alone resulted in tumour growth. Co-treatment with oestrogen plus progesterone resulted in a significant decrease in tumour volume, as compared to oestrogen alone, when measured by bioluminescence (Fig. 3a, b) ($P = 0.0021$) or tumour volume ($P = 0.019$) (Extended Data Fig. 6). Immunohistochemistry confirmed that PR expression was induced under both oestrogen and oestrogen plus progesterone conditions (Extended Data Fig. 7), but importantly, PR will only be active under dual hormone conditions.

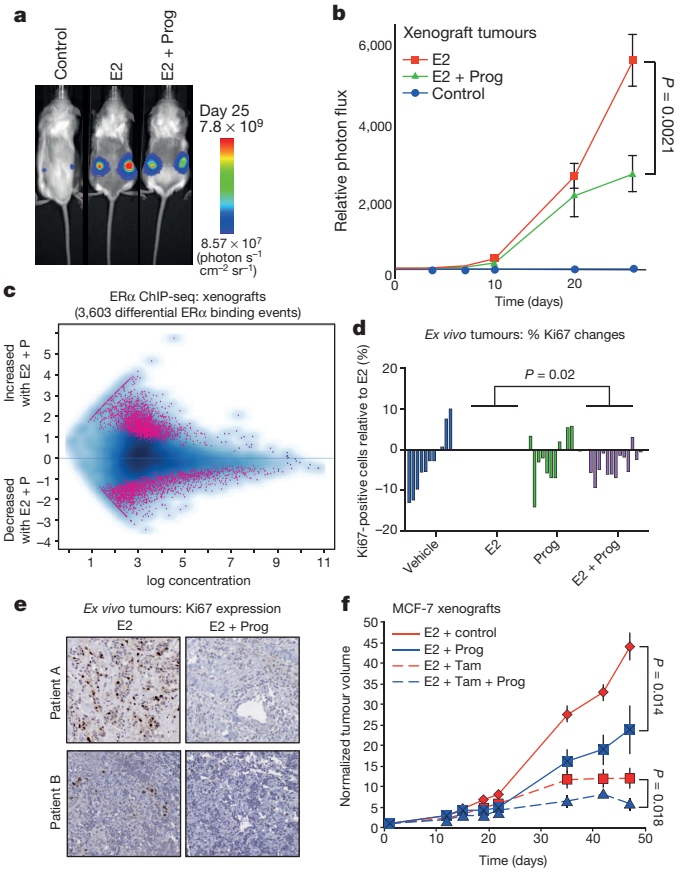

Figure 3 | Progesterone treatment inhibits ERα$^+$ tumour progression. **a**, MCF-7-Luciferase cells were implanted in NSG mice with control, oestrogen (E2) pellets or oestrogen plus progesterone (E2 + Prog) pellets ($n = 10$). **b**, Graphical representation of tumour formation, as assessed by bioluminescence. **c**, ERα ChIP-seq was conducted on randomly chosen ($n = 6$) xenograft tumours from ovariectomized NSG mice treated with oestrogen alone or oestrogen plus progesterone. MA (log ratios and means average) plot representing changes in ERα binding. **d**, Proliferative responses (Ki67 staining) of primary breast cancer tissues cultured *ex vivo* with oestrogen (E2) or progestin (R5020) alone or both in combination ($n = 14$ samples per treatment; except for vehicle ($n = 11$) and R5020 treatments ($n = 12$)). The *P* value was calculated using a linear mixed effect analysis. **e**, Representative images of Ki67 immunostaining in *ex vivo* cultured breast tumour tissue sections from two patients. **f**, MCF-7 xenografts were grown in NSG mice in the presence of oestrogen pellets. Mice were treated with vehicle, tamoxifen, progesterone or tamoxifen plus progesterone and normalized tumour volume is shown. The data were analysed using a *t*-test and the error bars represent ±s.e.m.

We repeated the MCF-7 xenograft experiment in ovariectomized mice, in order to eliminate any confounding issues related to endogenous mouse hormones. Assessment of tumour growth (Extended Data Fig. 7) confirmed the previous finding (Fig. 3b) that progesterone inhibited tumour formation. We performed ERα and PR ChIP-seq on six randomly selected sets of matched oestrogen or oestrogen plus progesterone stimulated xenograft tumours (taken from the final time point) and identified differentially bound ERα binding events. The major variable driving clustering of ERα binding events within tumour xenografts was the treatment condition (Extended Data Fig. 7). As observed in the short-term cell line experiments (Fig. 2), oestrogen-stimulated ERα binding in the xenograft tumours was substantially altered by progesterone treatment. We observed 3,603 differentially regulated ERα binding events in xenograft tumours from oestrogen plus progesterone conditions, when compared to oestrogen-only conditions (Fig. 3c). As such, progesterone induced a global reprogramming of ERα binding events *in vivo*, even following long-term hormonal treatment.

To extend our findings into primary tumours, we employed a novel *ex vivo* primary tumour culture system[27,28] to cultivate ERα$^+$ PR$^+$ primary tumours for short time periods, in order to study the effect of hormonal treatment on cell growth. Fourteen independent ERα$^+$ PR$^+$ primary tumours were used for the analysis. Each tumour was cut into small pieces and randomized onto gelatine sponges half-submersed in media to sustain tissue architecture and viability. Tumour explants were then cultivated under hormone-deprived conditions for 36 h, followed by a 48 h treatment with vehicle control, oestrogen, the synthetic progestin R5020 or oestrogen plus R5020. Tumours retained normal cellular and morphological features after treatment in the *ex vivo* context (Extended Data Fig. 8). Fixed tissues were stained for Ki67 to assess changes in proliferation. Most of the tumours responded to oestrogen with a coincident increase in the percentage of cells that expressed Ki67. Co-treatment with progestin significantly inhibited oestrogen-stimulated proliferation (Fig. 3d and Extended Data Fig. 8), showing that progesterone can antagonise oestrogen-induced growth in primary human breast tumours cultivated as explants. Example images are shown in Fig. 3e. Importantly, the addition of progestin alone did not increase growth rates (Fig. 3d and Extended Data Fig. 8), in support of our hypothesis that progesterone lacks proliferative potential and importantly, is anti-proliferative in an oestrogen-driven context. ERα and PR co-localization was confirmed in the explant tumour samples using immunofluorescence, as was the reduction in Ki67 following progestogen treatment (Extended Data Fig. 8).

Given our findings that progestogens are anti-proliferative in an oestrogen-driven tumour context, we combined progesterone treatment with a standard of care therapy in xenograft models. MCF-7 xenografts were implanted in NSG mice and supplemented with slow-release oestrogen pellets. Mice were subsequently treated with vehicle, progesterone alone, tamoxifen alone or progesterone plus tamoxifen and tumour growth was monitored. As previously seen (Fig. 3b and Extended Data Fig. 6), progesterone antagonised oestrogen-induced tumour formation, as did tamoxifen alone, but the combination of tamoxifen plus progesterone had the greatest tumour inhibitory effect (Fig. 3f). This experiment was repeated in a second xenograft model (T-47D cells), confirming the finding that tumour volume was inhibited by progesterone alone, but the greatest degree of tumour inhibition was observed under conditions where an ERα antagonist (tamoxifen) was coupled with a PR agonist (progesterone) (Extended Data Fig. 6).

PGR copy number alterations are common

Given the *PGR* copy number loss observed in the MCF-7 cell line (Extended Data Fig. 5), we explored whether this was a common phenomenon observed in breast cancer patients, by assessing genomic copy number alterations (CNA) within the METABRIC cohort of ~2,000 breast cancers[29]. This analysis revealed that 18.5% of all breast cancers possess a copy number loss in the *PGR* genomic locus and these are biased towards ERα$^+$ cases (Fig. 4a). This level of loss of heterozygosity (LOH) has been previously observed at this genomic locus in a small cohort of patients[30]. In total, 21% of ERα$^+$ breast cancers contain a heterozygous or a homozygous deletion of the *PGR* genomic locus and these tumours had significantly ($P < 0.001$) lower PR messenger RNA levels (Fig. 4b). Importantly, within the 1,484 ERα$^+$ cases, tumours with copy number loss of the *PGR* genomic region had a poorer clinical outcome ($P = 0.001$) (Fig. 4c), suggesting that inactivation of the *PGR* gene contributes to worse outcome within this subset of ERα tumours.

ERα mRNA levels are significantly higher in tumours with *PGR* copy number loss (Fig. 4d). Copy number loss of *PGR* affects gene expression events, since the expression level of genes shown to be progestogen-induced under oestrogenic conditions in the cell lines was significantly lower ($P < 0.001$) in tumours with *PGR* copy number loss and, inversely, the expression level

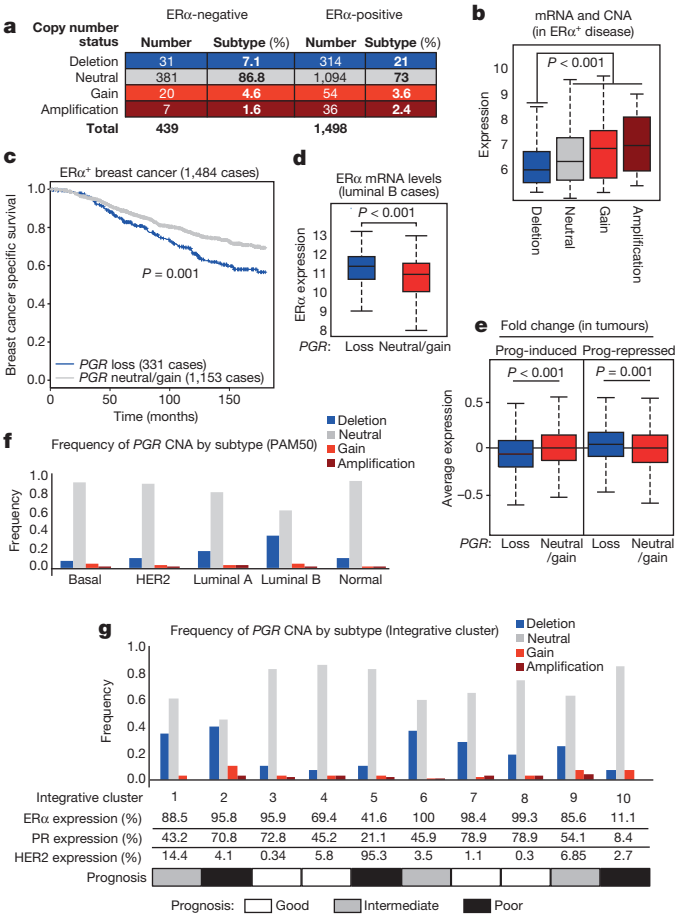

Figure 4 | The *PGR* genomic locus undergoes copy number loss in ERα$^+$ breast cancer. **a**, METABRIC breast cancers (1,937 in total) were assessed for copy number change in the *PGR* genomic locus. **b**, Correlation between PR mRNA levels and copy number status within all ERα$^+$ cases. The estimate of differences is 0.3551, 95% confidence interval: [0.244, 0.463]. **c**, Kaplan–Meier curve showing breast cancer specific survival in all ERα$^+$ cases. Cox model analysis: hazard ratio = 1.46 [1.156, 1.843]. **d**, Changes in ERα mRNA levels in luminal B tumours within the METABRIC cases. The estimate of differences is 0.4436, 95% confidence interval: [0.269, 0.618]. **e**, The expression levels of the stringent progestogen-induced or -repressed genes from the cell lines cultured under oestrogenic conditions were assessed in the ERα$^+$ METABRIC tumours. **f**, **g**, Relative fraction of tumours with *PGR* copy number alterations (can) events within molecular subtypes, based on the PAM50 gene expression profile (**f**) and the ten integrative clusters (**g**).

of genes repressed by progestogens in cell lines was significantly elevated ($P = 0.001$) in tumours with copy number loss of the *PGR* gene (Fig. 4e).

Using PAM50 breast cancer subtype stratification, 33% of luminal B tumours (typically poor prognosis and PR low/negative) possessed copy number loss of the *PGR* genomic region (Fig. 4f), explaining the lower PR protein levels in one third of this breast cancer subtype. In addition, even within the luminal A tumours only (which tend to have a better outcome), 19% have a copy number loss of *PGR* and this subset of luminal A tumours have a poorer clinical outcome (Extended Data Fig. 9). Tumours were then stratified based on the ten recently described genomic integrative clusters[29], revealing three ERα$^+$ subtypes (integrative clusters 1, 2 and 6) with at least 35% *PGR* copy number loss (Fig. 4g). All three of these integrative clusters have intermediate or poor clinical outcome (Fig. 4g). Data showing genomic copy number changes on the chromosome 11 arm that encompasses the *PGR* gene are shown in Extended Data Fig. 9. This level of *PGR* copy number loss was even higher in an independent cohort of breast cancer patients: 29% of luminal (ERα$^+$) breast cancers from

TCGA[31] (Extended Data Fig. 10). Within luminal B tumours only, 39% of TCGA breast cancer cases had a *PGR* copy number loss.

Our data show that PR and ERα are functionally linked in breast cancer cells with a greater complexity than previously recognized. Good prognosis luminal A ERα$^+$ PR$^+$ breast tumours, when exposed to both oestrogens and progestogens, have an ERα chromatin binding profile that is dictated by PR binding events. The functional significance of this steroid receptor crosstalk is regulation of a gene expression program associated with low tumorigenicity; hence, better disease outcome. Genomic alterations in the *PGR* genomic locus seem to be a relatively common mechanism for reduction of PR expression, which may consequently lead to altered ERα chromatin binding and target gene expression patterns that increase breast tumorigenicity and confers a poor clinical outcome. This ERα–PR crosstalk may be directly influenced by many variables, including the relative receptor levels and the hormonal milieu. The presence or absence of oestrogen may significantly alter the outcome of PR–ERα interactions, such that the antiproliferative effects of PR activation may be limited to oestrogenic conditions. Our findings show that PR is not simply a marker of a functional ERα complex[18]. Rather, we propose that PR is a critical determinant of ERα function owing to crosstalk between PR and ERα. In this scenario, under oestrogenic conditions, an activated PR functions as a proliferative brake in ERα$^+$ breast tumours by re-directing ERα chromatin binding and altering the expression of target genes that induce a switch from a proliferative to a more differentiated state[6].

Online Content Methods, along with any additional Extended Data display items and Source Data, are available in the online version of the paper; references unique to these sections appear only in the online paper.

Received 13 January; accepted 22 May 2015.
Published online 8 July 2015.

1. Chlebowski, R. T. *et al.* Estrogen plus progestin and breast cancer incidence and mortality in postmenopausal women. *J. Am. Med. Assoc.* **304,** 1684–1692 (2010).
2. Bentel, J. M. *et al.* Androgen receptor agonist activity of the synthetic progestin, medroxyprogesterone acetate, in human breast cancer cells. *Mol. Cell. Endocrinol.* **154,** 11–20 (1999).
3. Fournier, A., Berrino, F. & Clavel-Chapelon, F. Unequal risks for breast cancer associated with different hormone replacement therapies: results from the E3N cohort study. *Breast Cancer Res. Treat.* **107,** 103–111 (2008).
4. Blows, F. M. *et al.* Subtyping of breast cancer by immunohistochemistry to investigate a relationship between subtype and short and long term survival: a collaborative analysis of data for 10,159 cases from 12 studies. *PLoS Med.* **7,** e1000279 (2010).
5. Vignon, F., Bardon, S., Chalbos, D. & Rochefort, H. Antiestrogenic effect of R5020, a synthetic progestin in human breast cancer cells in culture. *J. Clin. Endocrinol. Metab.* **56,** 1124–1130 (1983).
6. Musgrove, E. A., Swarbrick, A., Lee, C. S., Cornish, A. L. & Sutherland, R. L. Mechanisms of cyclin-dependent kinase inactivation by progestins. *Mol. Cell. Biol.* **18,** 1812–1825 (1998).
7. Chen, C. C., Hardy, D. B. & Mendelson, C. R. Progesterone receptor inhibits proliferation of human breast cancer cells via induction of MAPK phosphatase 1 (MKP-1/DUSP1). *J. Biol. Chem.* **286,** 43091–43102 (2011).
8. Kabos, P. *et al.* Patient-derived luminal breast cancer xenografts retain hormone receptor heterogeneity and help define unique estrogen-dependent gene signatures. *Breast Cancer Res. Treat.* **135,** 415–432 (2012).
9. Zheng, Z. Y., Bay, B. H., Aw, S. E. & Lin, V. C. A novel antiestrogenic mechanism in progesterone receptor-transfected breast cancer cells. *J. Biol. Chem.* **280,** 17480–17487 (2005).
10. Bardou, V. J., Arpino, G., Elledge, R. M., Osborne, C. K. & Clark, G. M. Progesterone receptor status significantly improves outcome prediction over estrogen receptor status alone for adjuvant endocrine therapy in two large breast cancer databases. *J. Clin. Oncol.* **21,** 1973–1979 (2003).
11. Pichon, M. F., Pallud, C., Brunet, M. & Milgrom, E. Relationship of presence of progesterone receptors to prognosis in early breast cancer. *Cancer Res.* **40,** 3357–3360 (1980).
12. Badwe, R. *et al.* Single-injection depot progesterone before surgery and survival in women with operable breast cancer: a randomized controlled trial. *J. Clin. Oncol.* **29,** 2845–2851 (2011).
13. Bines, J. *et al.* Activity of megestrol acetate in postmenopausal women with advanced breast cancer after nonsteroidal aromatase inhibitor failure: a phase II trial. *Ann. Oncol.* **25,** 831–836 (2014).
14. Lee, Y. J. & Gorski, J. Estrogen-induced transcription of the progesterone receptor gene does not parallel estrogen receptor occupancy. *Proc. Natl Acad. Sci. USA* **93,** 15180–15184 (1996).
15. Dowsett, M. *et al.* Retrospective analysis of time to recurrence in the ATAC trial according to hormone receptor status: an hypothesis-generating study. *J. Clin. Oncol.* **23,** 7512–7517 (2005).
16. The Breast International Group (BIG) 1-98 Collaborative Group. A comparison of letrozole and tamoxifen in postmenopausal women with early breast cancer. *N. Engl. J. Med.* **353,** 2747–2757 (2005).
17. Viale, G. *et al.* Prognostic and predictive value of centrally reviewed expression of estrogen and progesterone receptors in a randomized trial comparing letrozole and tamoxifen adjuvant therapy for postmenopausal early breast cancer: BIG 1–98. *J. Clin. Oncol.* **25,** 3846–3852 (2007).
18. Cui, X., Schiff, R., Arpino, G., Osborne, C. K. & Lee, A. V. Biology of progesterone receptor loss in breast cancer and its implications for endocrine therapy. *J. Clin. Oncol.* **23,** 7721–7735 (2005).
19. Hurtado, A., Holmes, K. A., Ross-Innes, C. S., Schmidt, D. & Carroll, J. S. FOXA1 is a key determinant of estrogen receptor function and endocrine response. *Nature Genet.* **43,** 27–33 (2011).
20. Read, L. D., Snider, C. E., Miller, J. S., Greene, G. L. & Katzenellenbogen, B. S. Ligand-modulated regulation of progesterone receptor messenger ribonucleic acid and protein in human breast cancer cell lines. *Mol. Endocrinol.* **2,** 263–271 (1988).
21. Mohammed, H. *et al.* Endogenous purification reveals GREB1 as a key estrogen receptor regulatory factor. *Cell Rep.* **3,** 342–349 (2013).
22. Ballaré, C. *et al.* Two domains of the progesterone receptor interact with the estrogen receptor and are required for progesterone activation of the c-Src/Erk pathway in mammalian cells. *Mol. Cell. Biol.* **23,** 1994–2008 (2003).
23. Heintzman, N. D. *et al.* Histone modifications at human enhancers reflect global cell-type-specific gene expression. *Nature* **459,** 108–112 (2009).
24. Stark, R. & Brown, G. D. DiffBind: differential binding analysis of ChIP-Seq peak data. *Bioconductor* http://bioconductor.org/packages/release/bioc/html/DiffBind.html (2011).
25. Clarke, C. L. & Graham, J. D. Non-overlapping progesterone receptor cistromes contribute to cell-specific transcriptional outcomes. *PLoS ONE* **7,** e35859 (2012).
26. Liang, Y., Besch-Williford, C., Brekken, R. A. & Hyder, S. M. Progestin-dependent progression of human breast tumor xenografts: a novel model for evaluating antitumor therapeutics. *Cancer Res.* **67,** 9929–9936 (2007).
27. Centenera, M. M. *et al.* Evidence for efficacy of new Hsp90 inhibitors revealed by *ex vivo* culture of human prostate tumors. *Clin. Cancer Res.* **18,** 3562–3570 (2012).
28. Dean, J. L. *et al.* Therapeutic response to CDK4/6 inhibition in breast cancer defined by *ex vivo* analyses of human tumors. *Cell Cycle* **11,** 2756–2761 (2012).
29. Curtis, C. *et al.* The genomic and transcriptomic architecture of 2,000 breast tumours reveals novel subgroups. *Nature* **486,** 346–352 (2012).
30. Tomlinson, I. P., Nicolai, H., Solomon, E. & Bodmer, W. F. The frequency and mechanism of loss of heterozygosity on chromosome 11q in breast cancer. *J. Pathol.* **180,** 38–43 (1996).
31. Cerami, E. *et al.* The cBio cancer genomics portal: an open platform for exploring multidimensional cancer genomics data. *Cancer Discov* **2,** 401–404 (2012).

Supplementary Information is available in the online version of the paper.

Acknowledgements The authors would like to thank S. Leigh-Brown, the staff in the genomic core facility, S. Halim, the proteomic core facility and the bioinformatic core facility at Cancer Research UK. We acknowledge S. Jindal for pathology review, N. Ryan for technical assistance and S. Edwards for statistical analysis with *ex vivo* culture. The MCF7-LucYFP cells were a kind gift from N. Benaich. We thank H. Gronemeyer for the PR-A and PR-B expressing vectors. We would like to acknowledge the support of the University of Cambridge, Cancer Research UK and Hutchison Whampoa Limited. Research reported in this manuscript was supported by the National Cancer Institute of the National Institutes of Health under award number 5P30CA142543 (to University of Texas Southwestern) and Department of Defense grants W81XWH-12-1-0288-03 (GVR). W.D.T. is supported by grants from the National Health and Medical Research Council of Australia (ID 1008349; ID 1084416) and Cancer Australia (ID 627229) T.E.H. held a Fellowship Award from the US Department of Defense Breast Cancer Research Program (BCRP; W81XWH-11-1-0592) and currently is supported by a Florey Fellowship from the Royal Adelaide Hospital Research Foundation. J.S.C. is supported by an ERC starting grant and an EMBO Young investigator award.

Author Contributions Experimental work was conducted by H.M., I.A.R., T.E.H., G.A.T., A.A.A.S., A.B., A.S., C.D., J.L.L.R., R.L. and G.S. Computational analysis was conducted by R.S., O.M.R., S.M. and G.D.B. Clinical samples, information and support was provided by S.N.B., G.V.R., C.M.P. and C.C. *In vivo* work was conducted by J.S. Genomic work was conducted by J.H. and M.P. All experiments were overseen by W.D.T. and J.S.C. The manuscript was written by H.M., I.A.R., T.E.H., W.D.T. and J.S.C. with help from the other authors.

Author Information All microarray and ChIP-seq data are deposited in GEO with the accession number GSE68359. All proteomic data are deposited with the PRIDE database with the accession number PXD002104. Reprints and permissions information is available at www.nature.com/reprints. The authors declare no competing financial interests. Readers are welcome to comment on the online version of the paper. Correspondence and requests for materials should be addressed to J.S.C. (jason.carroll@cruk.cam.ac.uk) or W.D.T. (wayne.tilley@adelaide.edu.au).

METHODS

Cell lines and SILAC labelling of cell lines. MCF-7 and T-47D human cell lines were obtained directly from ATCC and grown in DMEM, supplemented with 10% FBS. All cell lines were regularly genotyped using STR profiling using the Promega GenePrint 10 system. Cell lines were regularly tested for mycoplasma infection.

Rapid IP-mass spectrometry of endogenous protein (RIME). Rapid immunoprecipitation- mass spectrometry experiments were performed as previously described[21]. MCF-7 and T-47D cells were grown in R/K-deficient SILAC DMEM (PAA; E15-086), 10% dialysed serum (Sigma-Aldrich; F0392), and supplemented with 800 mM L-lysine $^{13}C_6{}^{15}N_2$ hydrochloride and 482 mM L-arginine $^{13}C_6{}^{15}N_4$ hydrochloride (Sigma- Aldrich) for 'heavy'-labelled media or 800 mM L-lysine $^{12}C_6{}^{14}N_2$ hydrochloride and 482 mM L-arginine $^{12}C_6{}^{14}N_4$ hydrochloride for 'light'-labelled media. Antibodies used were against ERα (Santa Cruz - sc-543, lot- A2213) and PR (Santa Cruz- sc-7208, lot H2312). 20 μg of each antibody was used for each RIME experiment.

Each RIME experiment was performed by mixing 20 million cells from each label after respective drug treatments. Cells were treated with either progesterone (100 nM), R5020 (10 nM) or vehicle (ethanol). Two replicates of each experiment was performed and the results were validated by switching the SILAC labels. The RIME method, mass spectrometry and data analysis were performed as previously described[21].

Western blot and co-immunoprecipitation. Immunoprecipitation experiments for ERα and PR were performed using Santa Cruz antibodies. Antibodies used were against ERα (sc-543) and PR (sc-7208). Western blots for ERα and PR were performed using Novocastra antibodies (ERα: NCL-L-ER6F11 and PR: NCL-L-PGR-AB).

ChIP-seq. ChIP-seq experiments were performed as described[32]. Antibodies used were against ERα (Santa Cruz - sc-543, lot- A2213), PR (Santa Cruz- sc-7208, lot H2312) and p300 (Santa Cruz sc-585, lot –E2412). 10 μg of antibody was used for each experiment. Cells were treated with either progesterone (100 nM), R5020 (10 nM) or vehicle (ethanol) and experiment was performed in triplicates.

For xenograft experiments, ERα ChIP-seq experiments were performed from six sets of randomly chosen tumours under oestrogen only or progesterone and oestrogen treatment condition. Also included were two tumours from vehicle (control) conditions. Animals were randomly assigned to treatment groups using a random number generator at the beginning of the study.

ChIP-seq data analysis. Statistical tests and cut-offs were selected based on published recommendations[24].

RNA-seq. RNA-sequencing experiments were performed in MCF-7 and T-47D cells. Cells were treated with progesterone (100 nM) or R5020 (10 nM) for 3 h and RNA extracted. Experiment was performed in eight replicates for each cell line.

RNA-seq analysis. Single-end 40-bp reads generated on the Illumina HiSeq sequencer were aligned to the human genome version GRCh37.64 using TopHat v2.0.4 (ref. 33). Read counts were then obtained using HTSeq-count v0.5.3p9 (http://www-huber.embl.de/users/anders/HTSeq/doc/overview.html). Read counts were then normalized and tested for differential gene expression using the DESeq[34] workflow. Multiple testing correction was applied using the Benjamini–Hochberg method. Genes were selected as differentially expressed such that false discovery rate (FDR) <0.01.

GSEA analysis. Integration of the RNA-seq data and the ChIP-seq DBA results were carried out using gene set enrichment analysis (GSEA)[35] as follows. All genes assessed by RNA-seq were ranked and weighted by their mean $\log_2$ fold change on progesterone treatments. Lists of genes that overlapped with regions showing significant differential binding on progesterone treatment were derived. These data were then analysed using the GSEA v2.0.13 GSEA Preranked tool.

Gene signature analysis. We derive a prognostic gene signature of consisting of progesterone regulated genes. We included genes that were determined by RNA-seq (see above) as differentially upregulated in T47-D cells when subjected to progesterone/progestin, as well as having a differentially bound ER binding site with increased binding affinity (determined using DiffBind) within 10 kb of the transcription start site. 38 genes met these criteria (see Extended Data Fig. 5). This signature was validated using the METABRIC expression data set (15), showing that patients in the highest 10% of expression of genes in the signature exhibit significantly better breast cancer specific survival than patients in the lowest 10% of expression ($P = 7.36 \times 10^{-4}$); Extended Data Fig. 5).

As it has been shown that many gene signatures have significant power to predict outcome in breast cancer[36], we subjected the signature to additional statistical tests using the Bioconductor package SigCheck[37]. We used SigCheck to generate a null distribution of 1,000 signatures consisting of 38 genes selected at random, and computed their survival P values using the survival data for the 392 patients with high or low expression over the progesterone induced genes. The progesterone induced signature performed in the 99th percentile, with 1.2% of random signatures demonstrating an equal or lessor P value (empirical P value = 0.012; Extended Data Fig. 5). Considering previously identified cancer signatures, of the 189 oncogenic signatures identified in MSigDB[35], 11 had equal or lessor P values, placing the progesterone regulation signature in the 94th percentile (empirical P value = 0.058). All the code for analysis is available upon request.

Explant tissue experiments

Clinical samples. Breast tumour samples and relevant clinical data were obtained from women undergoing surgery at the Burnside Private Hospital, Adelaide, South Australia, with informed, written consent. This study was approved by the University of Adelaide Human Research Ethics Committee (approval numbers: H-065-2005; H-169-2011). Patients enrolled in the University of Texas, Southwestern study provided written consent allowing the use of discarded surgical samples for research purposes according to an Institutional Board-approved protocol. Tumours were obtained from the University of Texas, Southwestern Tissue Repository under Institutional Review Board (IRB) (STU 032011-187).

Tissue collection and processing. Excised tissue samples were delivered to the laboratory on ice within one hour following surgery and washed in culture medium comprised of phenol red-free RPMI (SAFC Biosciences, Kansas, USA), 200 mM glutamine (SAFC Biosciences), 1× antibiotic-antimycotic (Sigma-Aldrich), 10 μg/ml insulin (Sigma-Aldrich), and 10 μg/ml hydrocortisone (Sigma-Aldrich). Breast tumour tissues were cultured *ex vivo* as previously described[28]. In brief, tumour pieces (explants) were pre-incubated on gelatine sponges (3–4 per sponge) for 36 h in culture media containing 10% FCS, followed by treatment with hormones as indicated in culture media containing 10% steroid depleted FCS. The conditions used were: vehicle, oestradiol (10 nM), R5020 (10 nM) and the combination of oestradiol and R5020 (both at 10 nM) with hormone treatment conducted for 48 h. Representative pieces of tissue were fixed in 4% formalin in phosphate-buffered saline (PBS) at 4 °C overnight and subsequently processed into paraffin blocks. Sections (2 μm) were stained with haematoxylin and eosin and examined by a pathologist to confirm and quantify the presence/proportion of tumour cells.

Immunohistochemistry. Primary antibodies to detect ERα (ID5 1:300; DAKO M7047, Glostrup, Denmark), PR (1:1,000, Leica NCL-PGR-AB, Wetzlar, Germany) or Ki67 (MIB1 1:400; DAKO M7240 Glostrup, Denmark) were used in conjunction with a 1:400 dilution of a biotinylated anti-mouse secondary antibody for 30 min (DAKO E0433, Glostrup, Denmark) followed by incubation with horseradish peroxidase-conjugated streptavidin (DAKO P0397, Glostrup, Denmark). Visualization of immunostaining was performed using 3,3-diaminobenzidine (Sigma D9015), as previously described[38].

Image capture and quantification of Ki67 immunostaining. Slides were scanned at 40× magnification (NanoZoomer Microscopy System, Hamamatsu, Japan) and the digitized images edited to exclude non-glandular structures. A minimum of 10 high-resolution images from Nanozoomer files of all segments were recorded. Brown pixels (Ki67) and blue pixels (haematoxylin) were extracted from each image using Adobe Photoshop and the Colour Range tool and a fuzziness factor of 20. Extracted pixels were converted to greyscale format and a consistent threshold applied. Absolute numbers and proportion of Ki67-positive cells were determined using ImageJ software and the Analyse Particles tool with a circularity index of 0.2–1. An average of 14,000 cells were quantified per sample. Accuracy of automatic quantification was determined using an independent set of images that were assessed by an offsite independent observer who manually counted Ki67-positive and Ki67-negative cells in high-resolution images systematically sampled from an individual patient sample (containing >6,500 cells). Identical images were analysed by automatic quantification with consistency between manual and automatic counting of >95%. A linear mixed-effects model of percentage Ki67-positive cells versus type of treatment, adjusting for clustering on patient, was used to assess statistical significance.

Immunofluorescence. 5-μm sections were cut and adhered to Superfost UltraPlus slides (Menzel-Glasser Braunscweig, Germany) and baked on a warm block at 60 °C for 1 h. Sections were dewaxed in 3 × 5 min immersions of xylene followed by 3 × 5 min immersions in 100% ethanol. Sections were rehydrated in 2 × 5 min immersions in 70% ethanol followed by 2 × 5 min immersions in distilled H_2O. Next, antigen retrieval was performed in 600 ml of 1 mM Na-EDTA (pH 8.0) by heating in an 800 W microwave until boiling (approximately 5 min), allowing slides to stand for 5 min before microwaving at 50% power for an additional 5 min. Slides were allowed to cool in antigen retrieval buffer for 60 min before transferring to PBS for 5 min. Sections were encircled with a wax pen and primary antibody diluted in PBS with 10% normal goat serum was applied overnight at 4 °C (rat anti-ERα 1:100 (Abcam ab46186); mouse anti-PR 1:500 (Dako NCL-PGR-AB); rabbit anti-Ki67 1:100 (Abcam ab16667). Sections were washed twice for 5 min in PBS, followed by incubation with secondary antibody diluted (all at 1:400) in PBS with 10% normal goat serum for 30 min at room temperature (goat anti-rat Alexa488 (A11006); goat anti-mouse Alexa569 (A11031); goat

anti-rabbit Alexa647, (A21246.), Life Technologies). Sections were washed twice for 5 min in PBS, followed by incubation with 1 nM DAPI diluted in PBS for 2 min at room temperature. Sections were mounted under DAKO fluorescent mounting media (S3023) and each fluorescent channel captured separately using a Zeiss LSM700 confocal microscope.

***PGR* copy number analysis.** Matched DNA and RNA were extracted for 1,980 tumours. The copy number analysis was performed using the Affymetrix SNP 6.0 platform. The arrays were first pre-processed and normalized using CRMAv2[39] method from the aroma.affymetrix R package. For each array, allelic-crosstalk calibration, probe sequence effects normalization, probe-level summarization and PCR fragment length normalization were performed. Then the intensities were normalized against a pool of 473 normals for those samples that had no matched normal or against their matched normal when available. The log-ratios were segmented using the CBS algorithm[40] in the DNAcopy Bioconductor package. Then, callings into five groups (homozygous deletion, heterozygous deletion, neutral copy number, gain and amplification), were made using thresholds based on the variability of each sample and their proportion of normal contamination. Then, samples were classified as *PGR* loss if they showed any type of loss in any part of the gene.

RNA analysis was performed using Illumina HT-12 v3 platform and analysed using beadarray package[41]. BASH[42] algorithm was employed to correct for spatial artefacts. Bead-level data were summarized and a selection of suitable probes based on their quality was done using the re-annotation of the Illumina HT-12v3 platform[43]. The samples were classified into the five breast cancer subtypes using PAM50[44] and the 10 integrative clusters[29]. Two-sided *t*-tests were performed between expression values and loss of PGR to determine significance. Kaplan–Meier estimates and log-rank tests were obtained using the survival R package (http://CRAN.R-project.org/package=survival). Comparison of the expression of the stringent progesterone/R5020 induced or repressed genes in samples with PGR lost and not lost was performed averaging the expression of all the genes and running a two-sided *t*-test.

Xenograft experiments. Mice were maintained, and regulated procedures performed, according to UK Home Office project license guidelines. Sample size was calculated using a combination of the NC3Rs recommended Resource Equation method, and also prior knowledge of the experimental variability of breast cancer cell line xenografts in NSG animals. All *in vivo* experiments were performed using age matched female *NOD/SCID/IL2Rg*$^{-/-}$ (NSG) mice and all experiments were blinded. Animals were selected using the following criteria: sex (female) and age matched (where possible littermates were used) to reduce variability; only animals in excellent health were used (verified pathogen free and in excellent physical health); all animals were certified as NSG strain. Animals were randomly assigned to treatment groups using a random number generator at the beginning of the study. Briefly, mice were injected subcutaneously into the No. 4 inguinal mammary fat pad with a suspension of 10^5 MCF7-Luc2/YFP cells in 50% growth factor reduced Matrigel (BD Biosciences). Where appropriate, 90 day slow-releasing 17b-oestradiol (0.72 mg per pellet) and/or progesterone (10 mg per pellet) hormone pellets (Innovative Research of America) were implanted subcutaneously in recipient mice. Tumour growth was monitored using regular bioluminescent imaging (IVIS) and caliper measurement. Data were analysed using the GraphPad Prism statistical software package. Standard deviations within groups were similar and substantially less than the variation between the treatment groups. Sample size was determined by a pilot experiment with a smaller number of mice. Mice used for all experiments were age and litter matched (3 months) to reduce variability. 15 mice were injected with tumours and then 5 mice were selected at random for each treatment arm. Treatments were blinded using coded cages. Mice were regularly assessed for health and endpoint was determined on regulatory guidelines for tumour size.

For tamoxifen experiments, age-matched female NSG mice were injected as above with either 10^5 MCF7-Luc2/YFP cells or 10^7 T-47D-Luc2/mStrawberry cells in 50% growth factor reduced Matrigel (BD Biosciences). Concomitantly, a 90 day slow-release 17b-oestradiol (0.72 mg per pellet) (Innovative Research of America) was implanted subcutaneously. One week later either 90 day slow-release progesterone (10 mg per pellet) hormone or placebo pellets (Innovative Research of America) were implanted subcutaneously, and tamoxifen/vehicle administration was commenced. 100 µl tamoxifen (5 mg/mL) or vehicle (sterile filtered corn oil) were administered i.p. to a schedule of 3 days dosing/1 day rest for a total duration of 4 weeks (MCF7) or 8 weeks (T-47D). Tumour sizes were monitored as above. Each treatment arm consisted of 10 tumours.

For ovariectomy experiments, age matched female NSG mice were injected as before with 10^5 MCF7-Luc2/YFP cells in 50% growth factor reduced Matrigel (BD Biosciences), and 90 day slow-release 17b-oestradiol (0.72 mg per pellet) and/or progesterone (10 mg per pellet) and/or placebo hormone pellets (Innovative Research of America) were implanted subcutaneously in recipient mice. Concomitantly, ovariectomy was performed. Tumour sizes were monitored as above for 7 weeks. Each treatment arm consisted of 10 tumours.

32. Schmidt, D. *et al.* ChIP-seq: Using high-throughput sequencing to discover protein-DNA interactions. *Methods* **48,** 240–248 (2009).
33. Trapnell, C., Pachter, L. & Salzberg, S. L. TopHat: discovering splice junctions with RNA-Seq. *Bioinformatics* **25,** 1105–1111 (2009).
34. Anders, S. & Huber, W. Differential expression analysis for sequence count data. *Genome Biol.* **11,** R106 (2010).
35. Subramanian, A. *et al.* Gene set enrichment analysis: a knowledge-based approach for interpreting genome-wide expression profiles. *Proc. Natl Acad. Sci. USA* **102,** 15545–15550 (2005).
36. Venet, D., Dumont, J. E. & Detours, V. Most random gene expression signatures are significantly associated with breast cancer outcome. *PLOS Comput. Biol.* **7,** e1002240 (2011).
37. Stark, R. & Norden, J. Checking gene expression signatures against random and known signatures with SigCheck. *Bioconductor* http://www.bioconductor.org/packages/release/bioc/html/SigCheck.html.
38. Tilley, W. D. *et al.* Detection of discrete androgen receptor epitopes in prostate cancer by immunostaining: measurement by color video image analysis. *Cancer Res.* **54,** 4096–4102 (1994).
39. Bengtsson, H., Wirapati, P. & Speed, T. P. A single-array preprocessing method for estimating full-resolution raw copy numbers from all Affymetrix genotyping arrays including GenomeWideSNP 5 & 6. *Bioinformatics* **25,** 2149–2156 (2009).
40. Venkatraman, E. S. & Olshen, A. B. A faster circular binary segmentation algorithm for the analysis of array CGH data. *Bioinformatics* **23,** 657–663 (2007).
41. Dunning, M. J., Smith, M. L., Ritchie, M. E. & Tavare, S. beadarray: R classes and methods for Illumina bead-based data. *Bioinformatics* **23,** 2183–2184 (2007).
42. Cairns, J. M., Dunning, M. J., Ritchie, M. E., Russell, R. & Lynch, A. G. BASH: a tool for managing BeadArray spatial artefacts. *Bioinformatics* **24,** 2921–2922 (2008).
43. Barbosa-Morais, N. L. *et al.* A re-annotation pipeline for Illumina BeadArrays: improving the interpretation of gene expression data. *Nucleic Acids Res.* **38,** e17 (2010).
44. Parker, J. S. *et al.* Supervised risk predictor of breast cancer based on intrinsic subtypes. *J. Clin. Oncol.* **27,** 1160–1167 (2009).

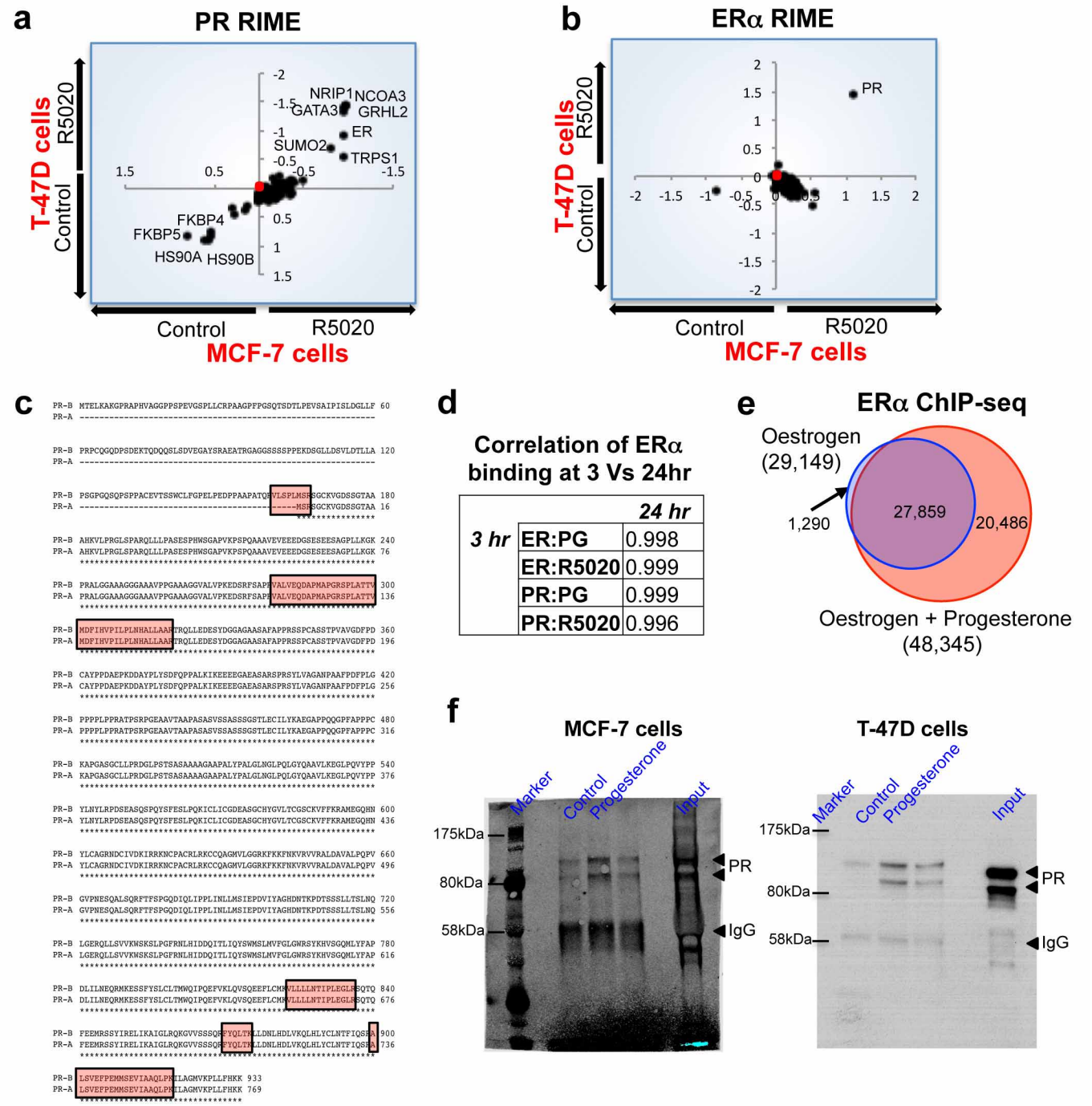

Extended Data Figure 1 | Protein purification of ERα and PR interacting proteins, using RIME, following treatment with a synthetic progestin. T-47D and MCF-7 breast cancer cells were grown in SILAC-isotope containing media and treated with either vehicle control or R5020, a synthetic progestin for 3 h. PR (**a**) or ERα (**b**) RIME was conducted and the proteins that were quantitatively enriched in both cell lines are shown. Only proteins that were enriched with a FDR < 1% were included. **c**, Peptide coverage of the PR protein following ERα RIME in T-47D cells. The identified peptides are highlighted and one of the peptides covers the 'Bus' region representing the PR-B isoform. **d**, Comparison of binding at different time points and treatment of MCF-7 breast cancer cells with progesterone. ERα ChIP-seq at 3 h and 24 h results in comparable binding. Correlation between progesterone (PG) and R5020 (RO) at 3 and 24 h. **e**, MCF-7 cells were grown in oestrogen rich complete media and treated with progesterone or vehicle control for 3 h. ERα ChIP was conducted and peaks that occurred in at least two of three independent replicates were considered. Venn diagram showing the changes in ERα binding following progesterone treatment of MCF-7 cells. **f**, Uncropped western blots from Fig. 1c.

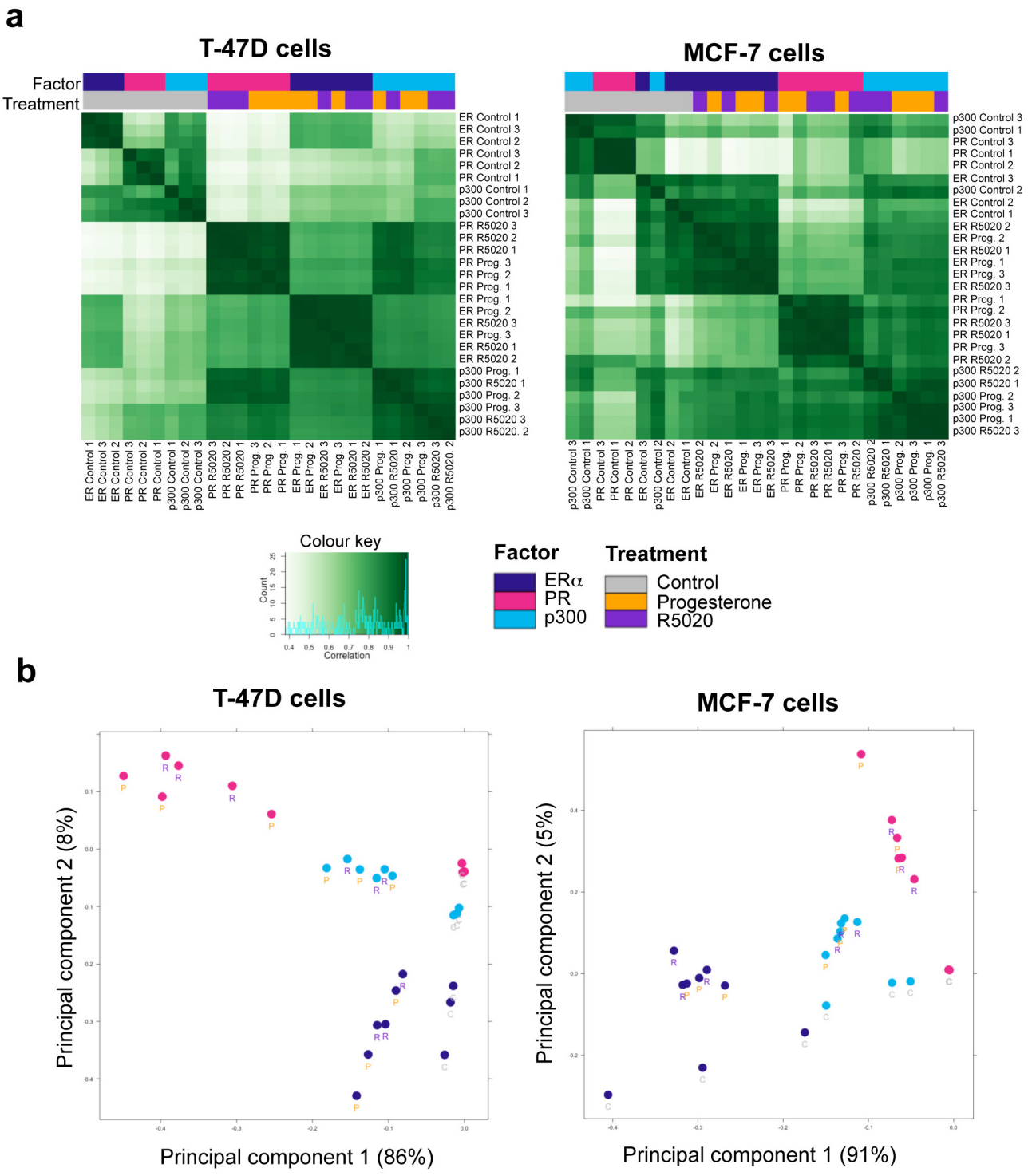

Extended Data Figure 2 | Clustering of ERα, PR, and p300 ChIP-seq experiments in two ERα$^+$ cell lines. For each experiment, all binding sites identified as overlapping in at least two samples are merged and retained, and normalized read counts computed at each site for each sample. **a**, Clustering correlation heat maps, based on Pearson correlations read scores (with replicate numbers in the labels), show good reproducibility between replicates and similarity of natural and synthetic hormone treatments. **b**, PCA plots showing the two most significant principal components (with samples labelled with treatment type: 'C' for full-media control conditions, 'P' for progesterone, and 'R' for R5020). The data from the two cell lines is shown.

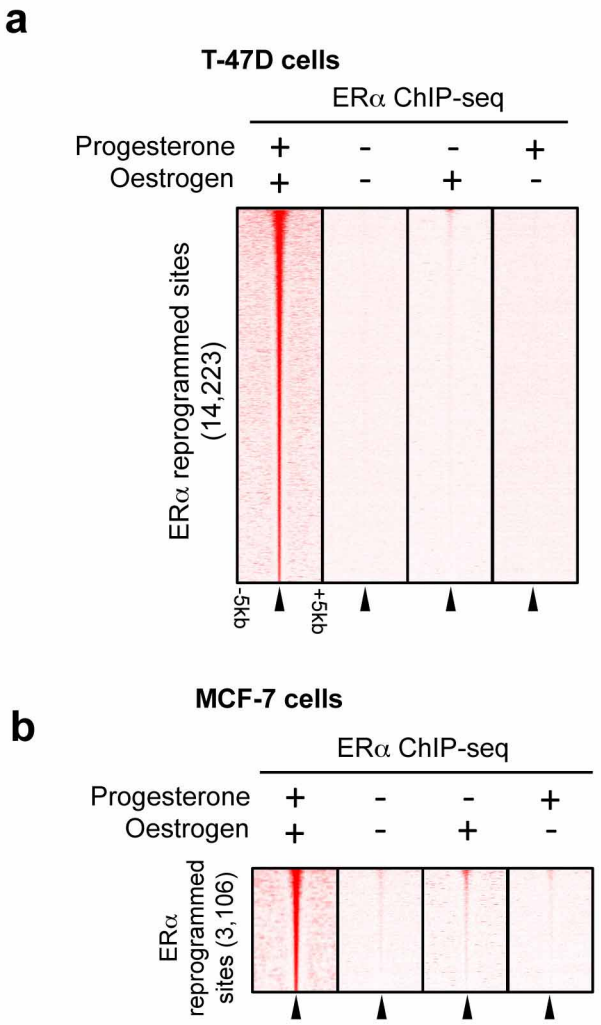

Extended Data Figure 3 | ERα binding in single hormone conditions. **a**, **b**, T47-D (**a**) or MCF-7 (**b**) cells were hormone-deprived and treated with vehicle control, oestrogen alone or progesterone alone. ERα ChIP-seq was conducted and we assessed the binding at the regions previously shown to be reprogrammed by oestrogen plus progesterone. The ERα reprogramming data under both oestrogen and progesterone conditions in the T-47D cells is from Fig. 2b. In the absence of oestrogen, progesterone does not induce ERα binding. In the absence of progesterone, oestrogen does not induce ERα binding to the locations shown to acquire reprogrammed ER binding events under dual hormone conditions.

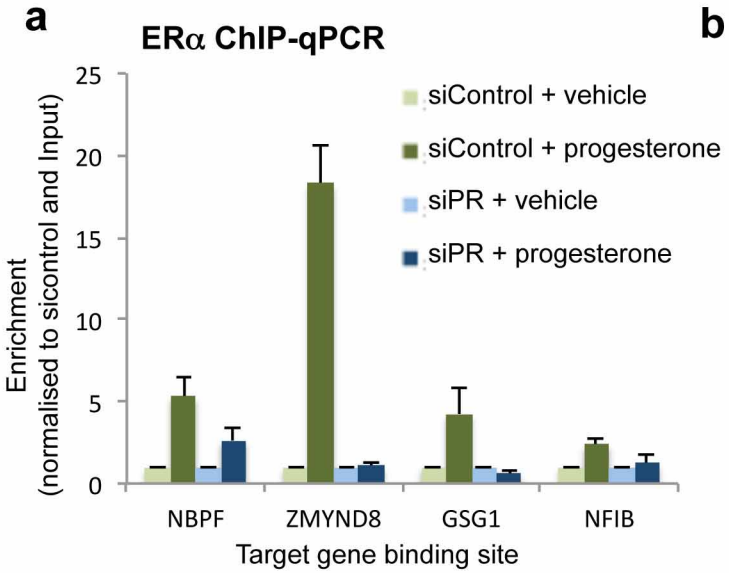

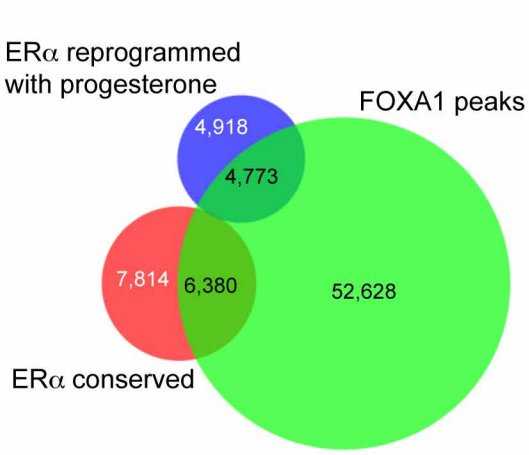

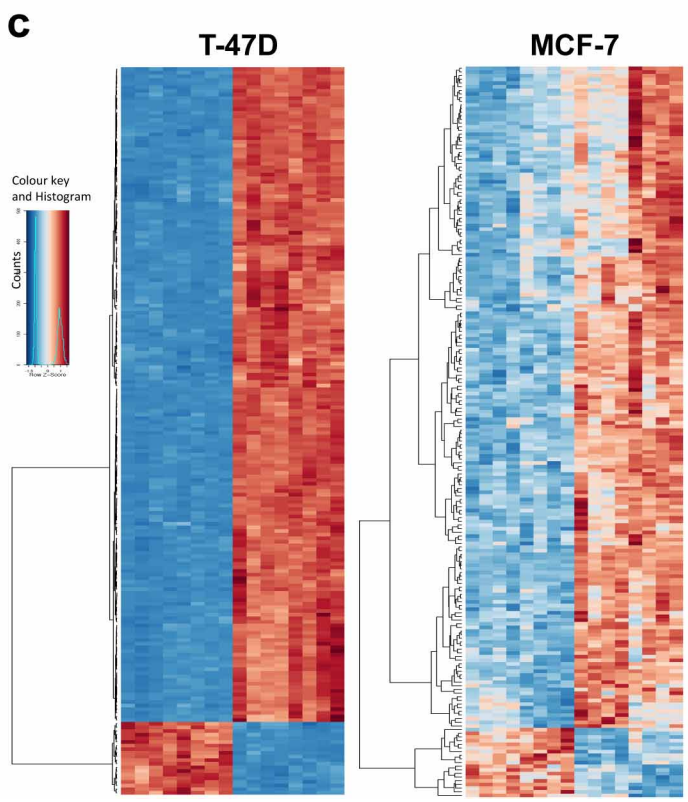

d

Cell line	Progesterone	R5020
T-47D	6,957	7,053
MCF-7	753	973
Both cell lines	543	718

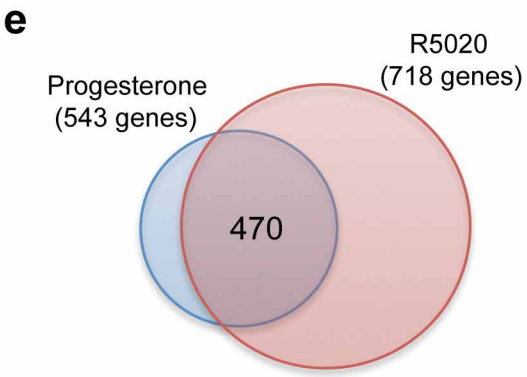

Extended Data Figure 4 | Validation of binding and gene expression changes. **a**, Validation of dependence on PR for ERα binding and overlap between ERα binding and FOXA1 binding. T-47D cells were grown in full, oestrogen-rich media and transfected with siControl or siRNA to PR. ERα ChIP was conducted followed by qPCR of several novel ERα binding events only observed under progesterone treatment conditions. In the absence of PR, ERα is not able to associate with the progesterone-induced binding sites. The figure represents one biological replicate of three completed replicates and the error bars represent standard deviation of the technical ChIP-PCR replicates. **b**, Venn diagram showing the ERα binding events that were conserved in T-47D cells (that is, not altered by progesterone when compared to oestrogen alone) and the ERα binding events that were reprogrammed by progesterone treatment, when overlapped with FOXA1 ChIP-seq data from T-47D cells. The FOXA1 ChIP-seq data from T-47D cells was from ref. 19. **c**, Differential gene changes in MCF-7 and T-47D cells following treatment with progesterone or R5020 for 3 h. Heat map showing gene changes relative to matched controls. Eight replicates were included. **d**, Table showing the differentially regulated genes in the two cell lines and in the two treatment conditions. **e**, Overlap between genes regulated by progesterone (in both cell lines) and gene regulated by the synthetic progestin R5020 (in both cell lines).

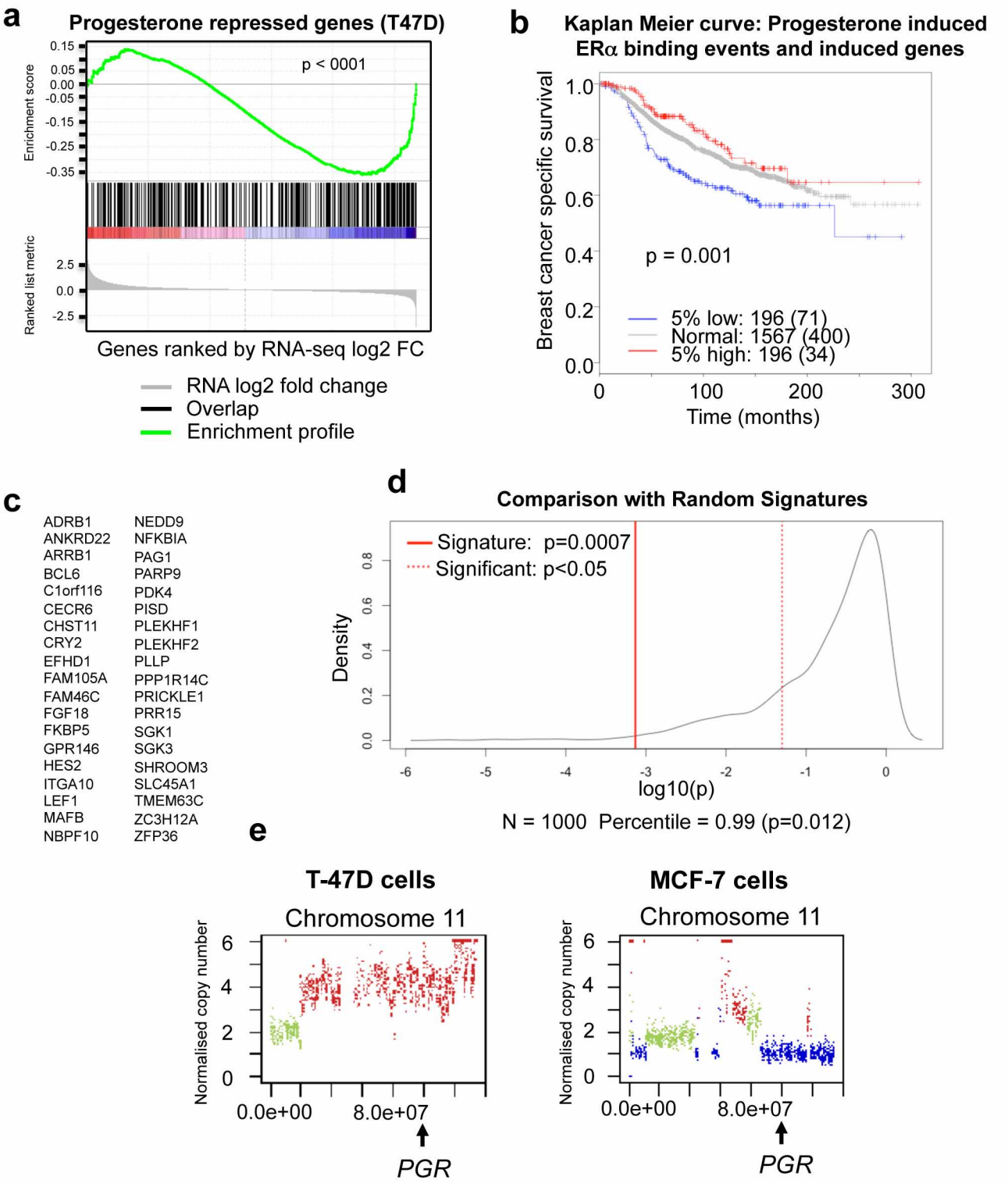

Extended Data Figure 5 | Analysis of gene expression changes and generation of gene signature. **a**, RNA-seq was conducted after progesterone or R5020 treatment for 3 h. GSEA analysis was conducted on progesterone/R5020 repressed genes with lost ERα binding events observed in T47-D cells. The progesterone-decreased ERα binding regions correlate with progesterone downregulated genes. **b**, Kaplan–Meier survival curve in 1,959 breast cancer patients based on a gene signature derived from the progesterone regulated genes and progesterone regulated ERα binding events. **c**, For a gene to be considered it was differentially regulated by progesterone/progestin (as measured by RNA-seq) and the gene had a differentially regulated ERα binding event within 10 kb of the transcription start site. This resulted in 38 genes. **d**, Performance of progesterone induced gene signature at separating based on survival over 392 patients in top or bottom 10% of expression compared to null distribution of *P* values computed using 1,000 randomly selected 38-gene signatures. **e**, Copy number alterations on chromosome 11 in T-47D and MCF-7 cells. Green is copy number neutral, blue is copy number loss and red is copy number gain. T-47D cells have an amplification of the chromosome 11 region encompassing the *PGR* gene and MCF-7 cells have a copy number loss of this genomic region.

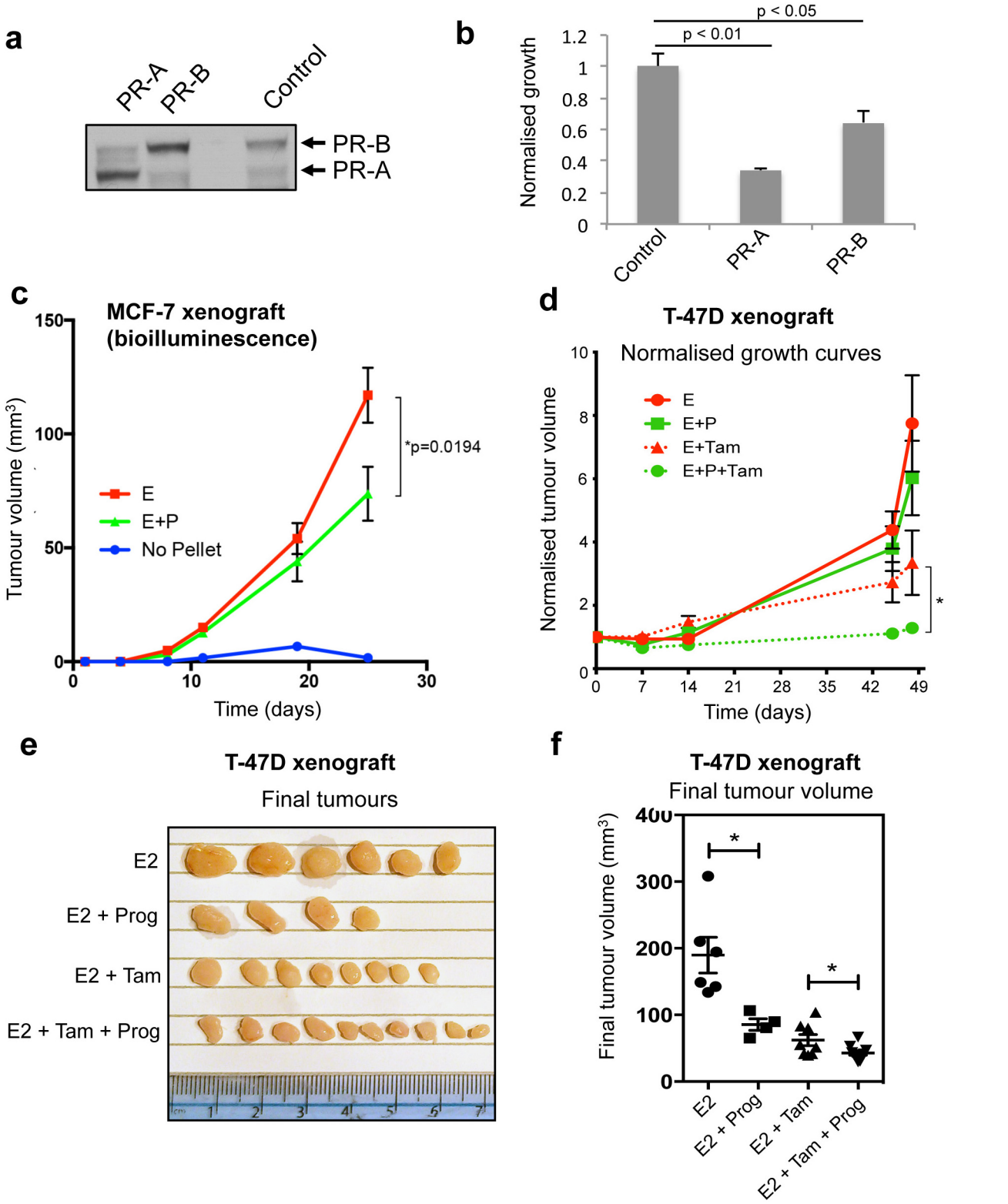

Extended Data Figure 6 | PR inhibits cell line growth and progesterone inhibits T-47D xenograft growth. **a**, MCF-7 cells were transfected with control vector, PR-A or PR-B expressing vectors. Western blotting confirmed the expression of the appropriate PR isoform. **b**, Growth was assessed following oestrogen plus progesterone treatment. The graph represents the average of three independent biological replicates and the error bars represent standard deviation. **c**, Assessment of MCF-7 xenograft tumour growth by physical measurement of tumour volume. Ten tumours for each condition (two in each of five mice per condition) were included. The data were analysed using a *t*-test and the error bars represent ±s.e.m. **d**, T-47D xenografts were established in NSG mice. Ten tumours for each condition (two in each of five mice per condition) were included. All were grown in the presence of oestrogen (E2) pellets and subsequently supplemented with vehicle, progesterone, tamoxifen or tamoxifen plus progesterone. Normalized tumour growth is shown. The data were analysed using a *t*-test and the error bars represent ±s.e.m. **e**, Final T-47D xenograft tumour volumes are shown. **f**, Final T-47D xenograft tumour volumes plotted graphically.

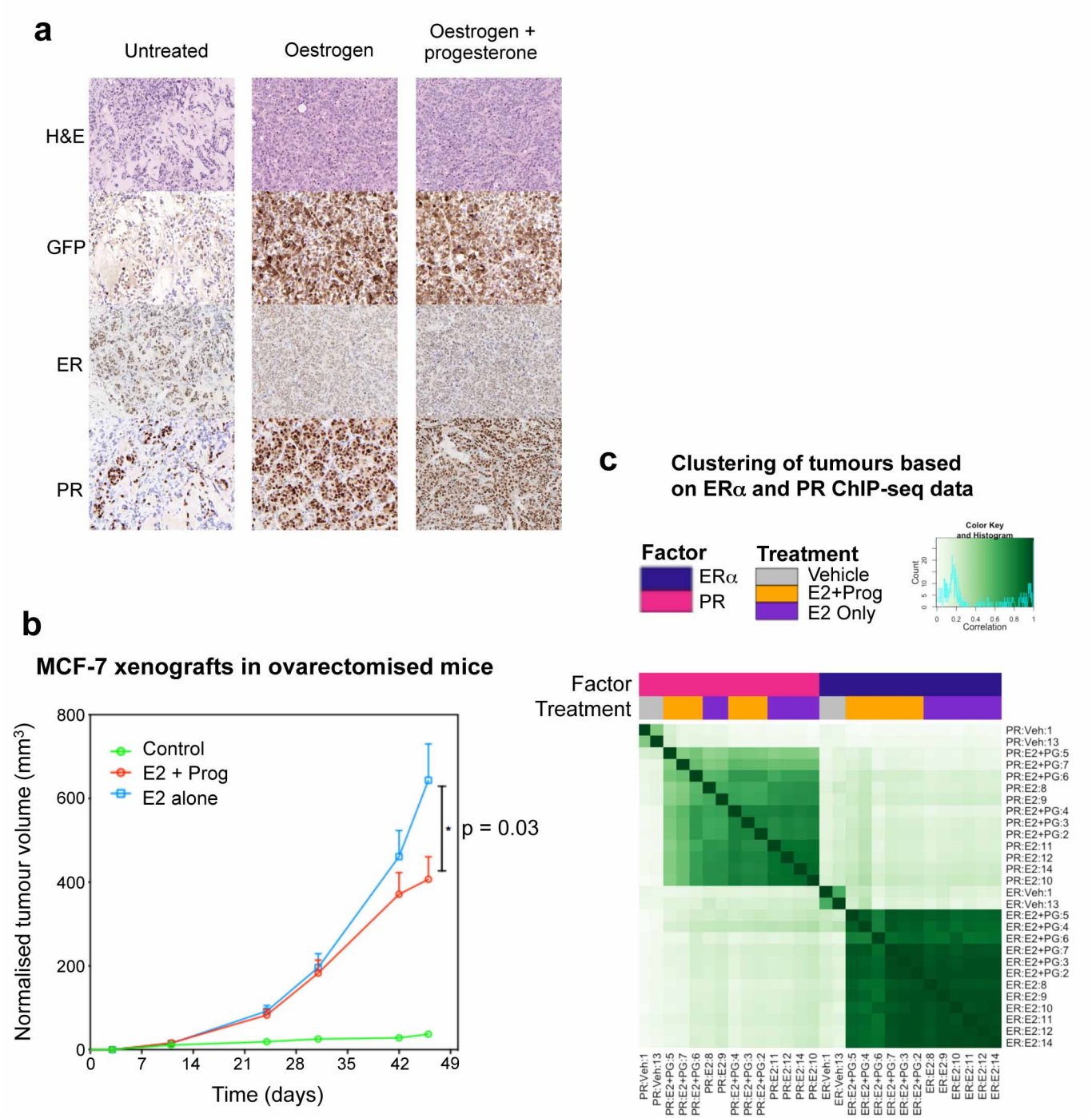

Extended Data Figure 7 | Histological analysis of xenograft tumours and ChIP-seq from xenograft tumours in ovariectomized mice. **a**, Histological analysis of MCF-7 xenograft tumours in untreated, oestrogen or oestrogen plus progesterone conditions. Tumours were taken from 25 day treated conditions. The human xenograft cells expressed GFP, permitting discrimination between human tumour cells and mouse host cells. MCF-7 xenograft experiment in ovariectomized mice. **b**, In order to map ERα binding events by ChIP-seq in MCF-7 xenograft tumours, we repeated the experiment in ovariectomized mice to eliminate any issues related to the endogenous mouse progesterone. Ten tumours for each condition (two in each of five mice per condition) were included. Growth of xenograft tumours under different hormonal conditions, Control, oestrogen alone (E2) and oestrogen plus progesterone (E2 + Prog). The data were analysed using a *t*-test and the error bars represent ±s.e.m. **c**, ChIP-seq for ERα and PR were conducted in six matched tumours from each hormonal condition. Also included were two tumours from no hormone conditions. Correlation heat map of all samples.

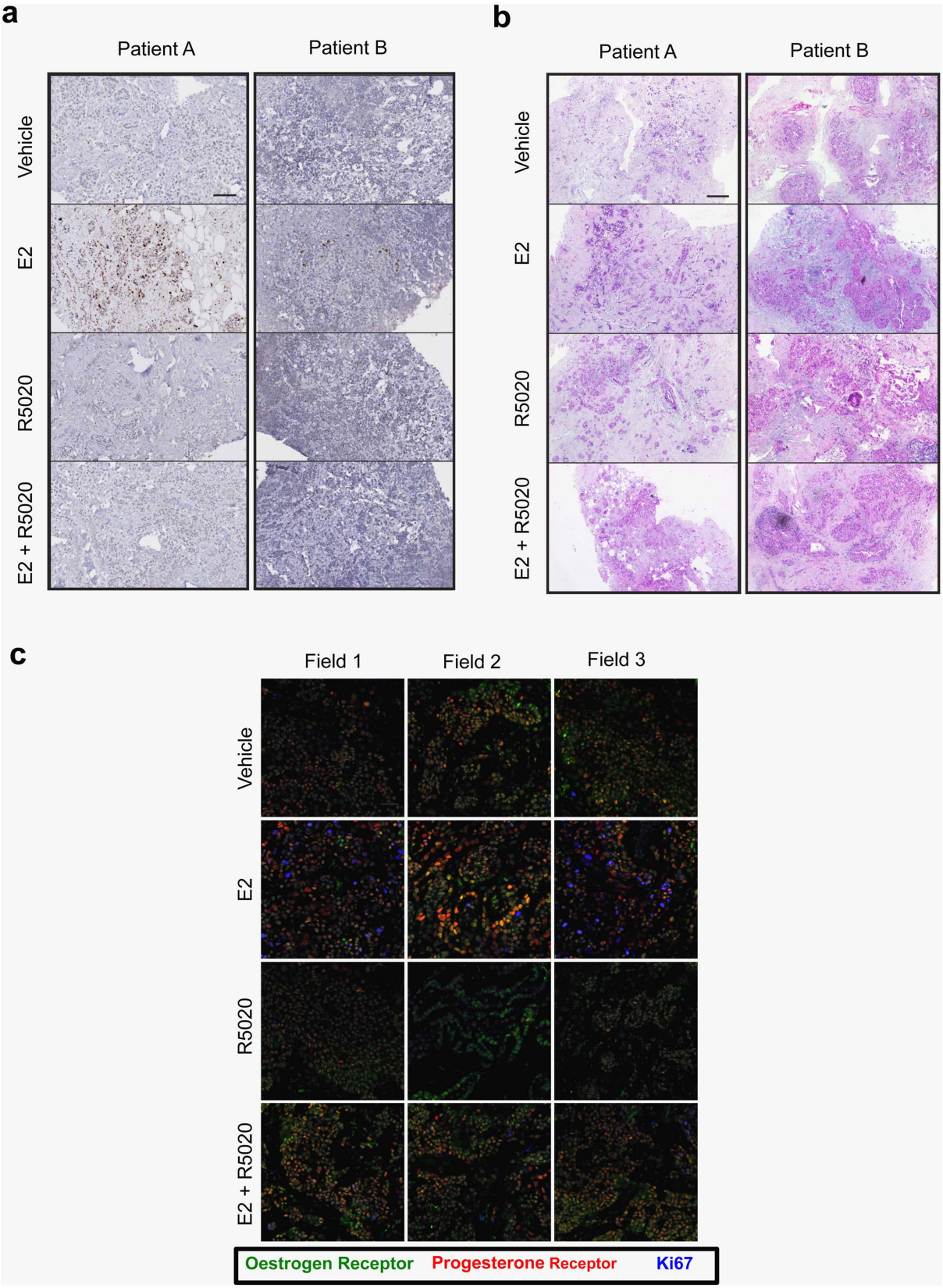

Extended Data Figure 8 | Primary tumours cultivated as *ex vivo* explants shown response to progesterone. Representative images of primary breast cancer explant tissue sections treated with vehicle, oestrogen (E2), the progestin R5020 or oestrogen plus progestin (E2 + R5020). **a**, **b**, These sections were probed with anti-Ki67 (brown) to label proliferating cells (**a**) or haematoxylin and eosin (**b**). Each image is of a single tissue segment from a selection of 3–4 sections per sample treatment. Scale bars, 100 μm. **c**, Confocal microscopy images (representative fields from each of the triplicate fragments) of a representative primary breast cancer explant tissue treated with vehicle, oestrogen (E2), the progestin R5020 (Progestin) or oestrogen plus progestin (E2 + R5020) and probed with anti-ERα (green), anti-PR (red) and anti-Ki67 to assess proliferating cells (blue).

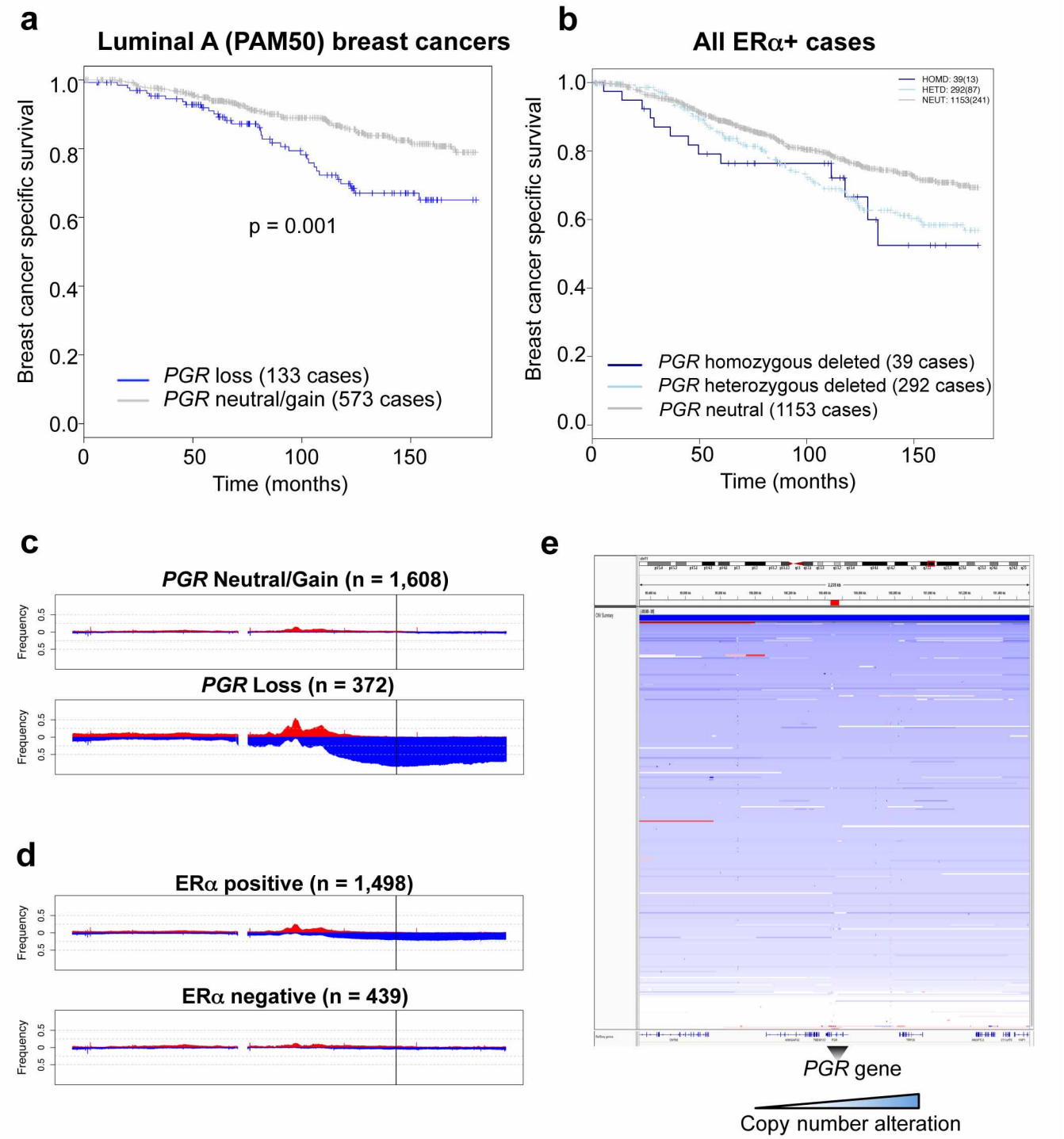

Extended Data Figure 9 | Analysis of *PGR* copy number loss in the METABRIC cohort. **a**, Kaplan–Meier analysis of breast cancer specific survival within the METABRIC cohort. Only within luminal A tumours (based on PAM50 gene expression signature), tumours were stratified based on copy number loss of *PGR* or not. In total 19% of luminal A tumours contain a copy number loss of the *PGR* genomic locus and these patients have a poorer clinical outcome. **b**, All ERα$^+$ cases were stratified based on *PGR* copy number status, showing tumours with heterozygous and homozygous deletions separately. **c**, Chromosome 11 in tumours with neutral or gained *PGR* versus those with copy number loss of the *PGR* gene (defined by line). **d**, Chromosome 11 copy number status between ERα positive and negative tumours. **e**, Visual representation of all ERα$^+$ tumours with a copy number alteration at the *PGR* genomic locus, showing the copy number changes relative to the *PGR* gene (highlighted below) and the surrounding ~2.2 Mb of genomic sequence.

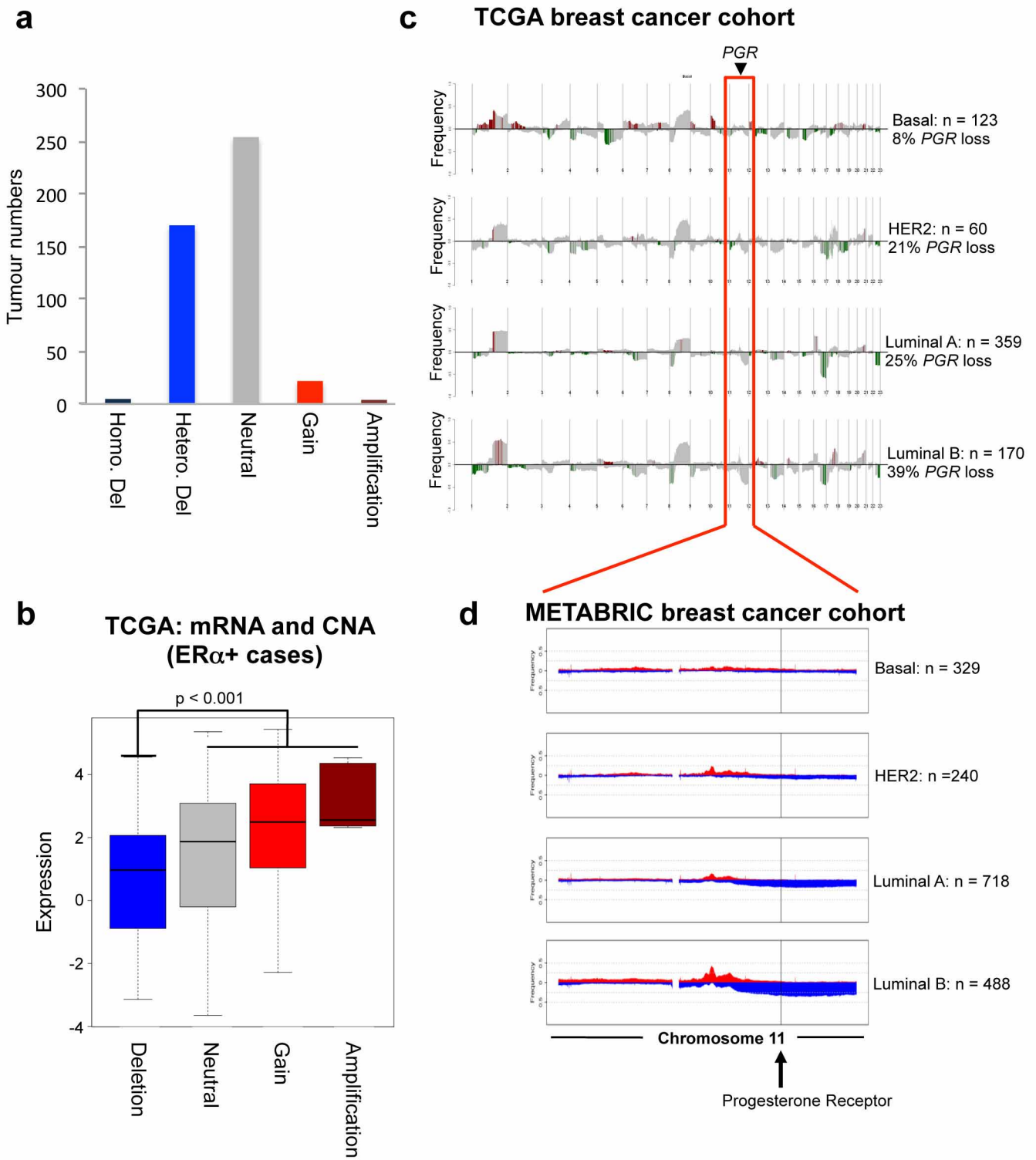

Extended Data Figure 10 | Validation of genomic copy number loss in the *PGR* gene in an independent data set. **a**, TCGA ERα^{+} breast cancers were assessed for copy number changes in *PGR*. The number of tumours in each category, based on copy number changes. Only ERα^{+} breast cancers were included. **b**, Correlation between PR mRNA levels and copy number status in all luminal breast cancers within the TCGA cohort. The heterozygous and homozygous deletions are combined. **c**, Frequency of copy number alterations across entire genome in TCGA breast cancer cohort, stratified based on subtype using PAM50 signature. Chromosome 11, which encompasses *PGR* gene is highlighted and the frequency of copy number loss of the *PGR* genomic region is provided. **d**, Copy number changes on chromosome 11 within the METABRIC cohort, based on subtype stratification (PAM50 signature).